CALCULATION OF DYNAMIC CHARACTERISTICS OF A FACE GAS-BARRIER IMPULSE SEAL FOR PUMP AND COMPRESSOR SHAFTS

EDUARD KUZNETSOV[1], ANTON PANDA[2], VOLODYMYR NAHORNYI[1]

[1] Sumy State University, Department of Information Technologies, Faculty of Electronics and Information Technologies, Sumy, Ukraine

[2] Technical University of Kosice, Department of Automotive and Manufacturing Technologies, Faculty of Manufacturing Technologies with a seat in Presov, Slovak Republic

DOI: 10.17973/MMSJ.2024_10_2024004

e-mail: **anton.panda@tuke.sk**

The article presents a combined mathematical model that allows us to determine and investigate the dynamic characteristics of the latest type of non-contact sealing for pump and compressor shafts, which eliminates leakage of pumped products, which are important from the point of view of safe operation. The proposed method is based on the laws of conservation of energy and conservation of matter. The model is based on static and dynamic calculation of operation characteristics, while its key feature is the combination of analytical, variational and numerical solutions. The materials of the article may be useful to developers of new types of contactless seals of centrifugal machines.

KEYWORDS

Impulse seal, barrier gas, face gap, mass flow rate of gas, boundary element method, dynamic characteristics, linearization of oscillation equations

1 INTRODUCTION

When designing modern pumps and compressors, special attention is paid to the safety of their operation. Today, these centrifugal machines are used to operate under operating conditions with a wide range of operating pressures and speeds. Also, the working conditions can be complicated by a high temperature difference: for example, transportation of high-temperature melts or maintenance of cryogenic equipment. In addition, the pumped product may have high toxic, radioactive or fire-hazardous properties. In this regard, the requirements for seals of such pumps and compressors are constantly being improved and tightened [Jurko 2011, Monkova 2013, Michalik 2014, Panda 2014 & 2021, Baron 2016, Mrkvica 2016, Macala 2017, Balara 2018, Duplakova 2018, Chaus 2018, Pandova 2018 & 2020, Sukhodub 2018 & 2019, Flegner 2019 & 2020, Harnicarova 2019].

The most suitable seals for the above operating conditions are seals in which a buffer medium is applied between the pumped product before seal and the atmosphere behind the seal. Excessive pressure of the buffer medium prevents leakage of the pumped product. Until recently, liquids neutral to the pumped product were used as a buffer medium. However, the ingress of such liquid into the casing of the pump or compressor leads to a violation of the purity of the pumped product. In addition, the cost of such a liquid and the system of its storage, preparation and supply to the seal increases the cost of pumping the product. In recent decades, a product-neutral gas (for example, air, nitrogen, argon) has been used as a buffer medium in seals. This made it possible to significantly simplify the buffer medium supply system, since the compressibility of the gas allows it to accumulate in large quantities and be fed into the seal without significant energy expenditure. In addition, the use of gas has significantly expanded the temperature range of the seals.

Seals using gas as a buffer medium in most cases operate in non-contact mode, that is, the movable and fixed parts of the seal do not touch during operation. This mode of operation is provided by gas-static or gas-dynamic effects in the separation zone between the movable and fixed parts of the seal (in the operation gap). These effects occur due to the special design of the sealing ring surfaces forming the operation gap. Usually such surfaces have either special channels for supplying gas to the operation gap, or special spiral grooves that capture gas from the supply zone and move it into the operation gap (in the second case, seals with a double set of sealing rings and gas supply to the zone between them are used). The most effective seals common today are gas dynamic seals with a double set of sealing rings. The cost of such seals is the highest of the existing ones due to the complexity of manufacturing surfaces with gas-dynamic grooves.

The article considers a new type of seal, which uses both gas-static and gas-dynamic effects in the working gap, but uses one pair of sealing rings, and the design of the sealing ring surfaces does not contain gas-dynamic grooves [Zaborowski 2007, Adamcik 2014, Svetlik 2014, Rimar 2016, Olejarova 2017 & 2021, Sedlackova 2017, Catlos 2018, Labun 2018, Gamec 2019, Kuznetsov 2019, Murcinkova 2019, Pollak 2019 & 2020, Straka 2021 & 2022, Vagaska 2021].

2 RESEARCH METHODOLOGY

In this section, we will consider a mathematical model of a gas dynamic impulse seal with buffer gas supply directly into the operation gap. (Fig. 1).

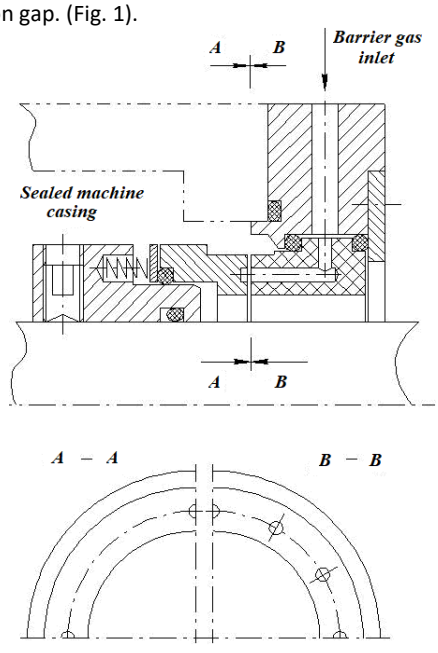

Figure 1. The design of the gas-barrier-impulse seal

During the operation of the seal, under the action of a combination of forces applied to the end and back surfaces of the axially movable sealing ring, the latter shifts and occupies a position in which the sum of the forces acting on its end surface F_s is balanced by the sum of the forces acting on the back surface F_c. The equation of axial vibrations of a movable o-ring has the form:

$$m\ddot{x}+c\dot{x}+k(\Delta+x)=F. \quad (1)$$

where x, $\dot{x}$ и $\ddot{x}$ are, respectively, the displacement, displacement velocity and acceleration of the axially movable sealing ring; m is the mass of the ring; c is the coefficient of resistance to movement equal to the dynamic viscosity of the gas with which the ring contacts; k is the stiffness of the springs; Δ is the pre–compression of the springs; $F=F_s-F_c$ is the resultant of the forces acting on the ring F_s and F_c, the values of which are determined by the pressure diagrams acting on the corresponding sites of the ring (Fig. 2).

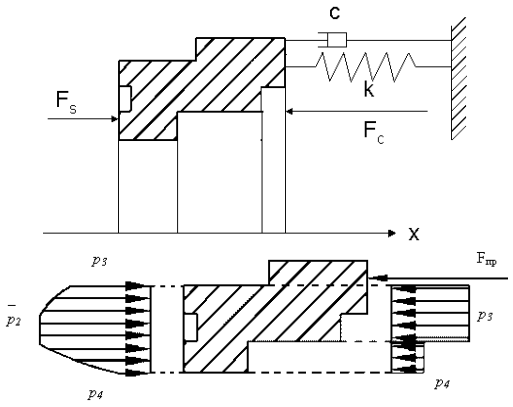

Figure 2. The scheme for calculating the seal and the plot of the load on the ring design of the gas-barrier-impulse seal

To solve (1), the equation of the sealing workflow is additionally considered – the balance of mass gas flow through the seal gap with a central angle equal to the angular size of the chamber on the surface of the sealing ring (Fig. 3).

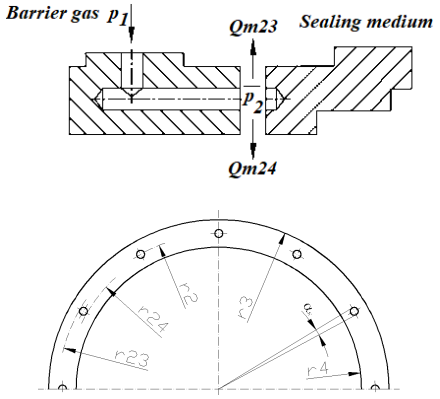

Figure 3. The flow diagram of the gas and the design of the sealing ring with chambers in the gas barrier impulse seal

During the operation of the seal, the barrier gas enters the chamber only when it communicates with the supply channel, therefore, the balance of gas flow from the chamber into the sealed gap and into the atmosphere will be determined by the expression:

$$Q_{m12}\,t_2=Q_{m23}\,(T-t_2)+ Q_{m24}\,(T-t_2)+Q_{\Delta V}+Q_{\Delta p}. \quad (2)$$

where Q_{m23} is the mass flow rate of the barrier gas from the chamber into the sealed casing through an external throttle with a central angle α_k, limited by radii r_3 and r_{23} during time $T-t_2$; Q_{m24} is the mass flow rate of the barrier gas from the chamber into the environment through an internal throttle with an angle α_k, radii r_{24} and r_4 during time $T-t_2$; $Q_{\Delta V}$ is the flow rate to displace gas from the gap; $Q_{\Delta p}$ – the flow rate for compressing gas in the chambers when the pressure changes caused by gap width fluctuations; Q_{m12} – the flow rate for compressing gas in a closed chamber during gas injection from the supply channel into the chamber during t_2; T is the time between two consecutive coincidences of the chamber with the supply channel; t_2 is the time during which the chamber is connected to the supply channel (the time when the chamber is filling with barrier gas).

The gas flow balance equation is written in terms of the geometric characteristics of the end gap [Kuznetsov, 2023]:

$$g_{m12}\,(p_1-\bar{p}_2)=g_{m23}(\bar{p}_2^2-p_3^2)+ +g_{m24}(\bar{p}_2^2-p_4^2)+g_{mV}\dot{x}+g_{mp}\dot{\bar{p}}_2. \quad (3)$$

where $g_{m23}(r_3,r_{23},x,\alpha_k,\mu)$ and $g_{m24}(r_4,r_{24},x,\alpha_k,\mu)$ are the conductivities of the external and internal throttles, respectively (gap sections bounded by radii r_3 and r_{23}, and radii r_{24} and r_4); $g_{m12}(V_k,T)$, $g_{mV}(r_3,r_4,T)$ and $g_{mp}(V_k,T)$ are the "conductivities" of the chamber and gas displacement from the gap.

The equation of the dynamics of the system can be obtained by combining equations (1) and (3) into a dimensionless dependence. For this purpose, the basic values of the gap $x=x_b$, the pressure of the sealing medium $p_1=p_b$ and the angular velocity $\omega=\omega_b$ at the nominal operating mode of the seal are entered into the calculation. Then, expressing the conductivities in terms of the base values, we can write:

$$g_{m12b}\,\Omega(\psi_1-\psi_2)=g_{m23b}\,u^3\left(\psi_2^2-\psi_3^2\right)+ +g_{m24b}\,u^3\left(\psi_2^2-\psi_4^2\right)+g_{m\Delta Vb}\cdot\dot{u}+g_{m\Delta pb}\cdot\dot{\psi}_2 \quad (4)$$

where $\psi_1=p_1/p_b$, $\psi_2=\bar{p}_2/p_b$, $\psi_3=p_3/p_b$, $\psi_4=p_4/p_b$ are the dimensionless pressures of the barrier gas, in the chambers, in the sealed machine casing and behind the seal, respectively.

It is possible to extend the validity (4) to the sections of the gap between the chambers. Then, as $\bar{p}_2$, it is necessary to use the pressure value averaged per revolution in the chamber and in the gap between it and the adjacent chamber. To find $\bar{p}_2$ in the gaps between the chambers, a numerical solution of the Reynolds equation, widely known from the theory of hydrodynamic lubrication, was used, which relates the pressure function of a lubricant to the thickness of its layer, its viscosity, density, and velocity of one of the surfaces bounding the lubricating layer:

$$\frac{\partial}{\partial y}\left(\rho x^3\frac{\partial p}{\partial y}\right)+\frac{\partial}{\partial z}\left(\rho x^3\frac{\partial p}{\partial z}\right)= =6\mu\frac{\partial(pxU)}{\partial y}+12\mu\frac{\partial(px)}{\partial t} \quad (5)$$

Due to the nonlinearity of equation (5), its analytical integration in a general form is currently not possible. Its numerical solution is performed by the modern numerical method of boundary elements. Expressing $\rho=p^{\kappa}$ (κ is the polytrope

index) and assuming, as a first approximation, that the gas flow regime in the gap does not change with time ($\partial P/\partial t = 0$), we can rewrite (5) as:

$$\frac{\partial}{\partial y}\left(x^3 \frac{\partial p^{\left(1+\frac{1}{\kappa}\right)}}{\partial y} \right) + \frac{\partial}{\partial z}\left(x^3 \frac{\partial p^{\left(1+\frac{1}{\kappa}\right)}}{\partial z} \right) = 6\left(\frac{1}{\kappa}+1\right)\frac{\partial}{\partial y}\left(U p^{\frac{1}{\kappa}} x \right) \quad (6)$$

To find a solution to this Poisson equation, you can use the following method: find a solution (6) without the right side (in the form of the Laplace equation), and then subtract a partial solution (the right side) from the resulting general solution, independent of boundary conditions. It is possible to bring (6) to the Laplace equation by assuming that the gas flow regime in the gap is only radial, i.e. due to the pressure difference between the outer and inner radii of the gap. The unknown quantities in it will be the desired function $P = p^{1+1/\kappa}$ and the value of the gap x, which, in turn, changes little in the circumferential and radial directions and can be considered unchanged in the first approximation. Thus, it is possible to write:

$$\frac{\partial^2 P}{\partial y^2} + \frac{\partial^2 P}{\partial z^2} = 0 \quad (7)$$

The essence of the applied numerical method consists in reducing the boundary value problem for partial differential equation (6) to an integral equation along the boundary of the studied region, which is obtained by applying the third Green formula to the desired function. In general, the integral equation for a region with a boundary Γ has the form [Kuznetsov, 2020]:

$$c(\xi)P(\xi) + \int_\Gamma P(\zeta)\, q^*(\xi,\zeta)\, d\Gamma(\zeta) = \int_\Gamma q(\zeta) P^*(\xi,\zeta)\, d\Gamma(\zeta) \quad (8)$$

where ξ is an arbitrary point on the boundary of the region, $c(\xi)$ is a function that takes into account the features that arise when integrating along the boundary of the region, $P^*(\xi,\zeta) = (1/2\pi)\ln(1/r)$ is the fundamental solution of the Laplace equation for the two-dimensional case, r is the distance between points ξ and ζ on the boundary of the region, $q^*(\xi,\zeta) = \partial P^*(\xi,\zeta)/\partial n(\zeta)$.

The solution of equation (7) is carried out by dividing the boundary of the region into sections (elements), the integration of which is performed numerically by the method of Gauss mechanical quadratures. Thus, a system of linear algebraic equations is obtained, the solution of which is carried out by the Gauss method. As a result of its solution, unknown values of functions P and $\partial P/\partial n$ at the boundary are determined, knowing which it is possible to determine the values of the pressure function at any i-th point inside the area surrounded by the boundary Γ:

$$P_i = \int_\Gamma q P^*\, d\Gamma - \int_\Gamma P q^*\, d\Gamma \quad (9)$$

As an area for determining the gas pressure field, a section of the gap is selected, limited by the outer and inner radii of the sealing ring and radial secants passing through the middle of the adjacent chambers (Fig. 4). The pressure functions are set as boundary conditions: at the outer radius – p_3, at the inner radius – p_4, in the zones of the supply channels – p_1; along the radius, the pressure varies according to the quadratic law (isothermical flow).

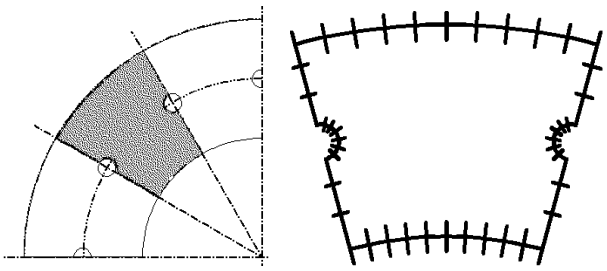

Figure 4. Allocation and division into elements of the calculation area

The integral equation (7) is given a discrete form, and the boundary of the region is divided into N elements, on each of which a Dirichlet type boundary condition is set – the pressure value (Fig. 4):

$$\frac{1}{2}P_i + \sum_{j=1}^{N}\left(\int_{\Gamma_j} q^*\, d\Gamma\right) P u_j = \sum_{j=1}^{N}\left(\int_{\Gamma_j} P^*\, d\Gamma\right) q_j \quad (10)$$

Integrals $\int_{\Gamma_j} q^*\, d\Gamma$ and $\int_{\Gamma_j} P^*\, d\Gamma$ establish a connection between the i-th node and the j-th element, along the length of which the integral is taken, and will henceforth be denoted respectively H_{ij} and G_{ij}. Integrals H_{ij} and G_{ij} are calculated using Gauss quadrature formulas for the elements. Hence, a relation is obtained that represents the relationship between the inner point i and the values of P and q at the boundary of the region:

$$P_i = \sum_{j=1}^{N} G_{ij} q_j - \sum_{j=1}^{N} H_{ij} P_j \quad (11)$$

Finding the right side of equation (6) $W(y) = 6(1+1/\kappa)\cdot\partial\left(U p^{1/\kappa} x\right)/\partial y$ is carried out by successive iterations: the value of the derivative $\partial P/\partial y$ found from (7) is substituted into the integral equation (8) in the form of $\int_\Omega W(y) P^*(\xi,\zeta)\, d\Omega(\zeta)$ (the derivative is easily determined by the finite difference method). After the values of the functions P and q are found on the entire boundary, P is calculated at an arbitrary inner point using the expression:

$$P_i = \sum_{j=1}^{N} G_{ij} q_j - \sum_{j=1}^{N} H_{ij} P_j - B_i \quad (12)$$

where B_i is the numerical solution of $W(y)$ for each value of the fundamental solution given in the i-th node.

Applying (12) to the entire study area, an array of barrier gas pressure values between adjacent chambers and supply channels was obtained to calculate the value of the averaged pressure $\bar{p}_2$ on the end belt where the chambers are located (limited by radii r_{24} and r_{23}).

Expressions for the forces acting on the sealing ring in dimensionless form:

$$\varphi_s = \frac{F_s}{p_b S_b} = \\ = \frac{2}{3}\frac{\psi_2^3 - \psi_3^3}{\psi_2^2 - \psi_3^2}\frac{S_{23}}{S_b} + \psi_2\frac{S_{22}}{S_b} + \frac{2}{3}\frac{\psi_2^3 - \psi_4^3}{\psi_2^2 - \psi_4^2}\frac{S_{24}}{S_b} \quad (13)$$

$$\varphi_c = \frac{F_c}{p_b S_b} = \psi_3\frac{S_{35}}{S_b} + \psi_4\frac{S_{54}}{S_b} + \lambda$$

where S_{ij} is the area of the corresponding throttling belts; λ is the dimensionless compression force of the springs.

$$\begin{aligned}&\left(g_{m12b}\psi_{10} - g_{m12b}\psi_{20}\right)\delta\Omega - \left(g_{m12b}\Omega_0\right)\delta\psi_1 + \\ &+\left(g_{m12b}\Omega_0\right)\delta\psi_2 = (3g_{m23b}u_0^2\psi_{20}^2 - 3g_{m23b}u_0^2\psi_{30}^2 - \\ &-3g_{m24b}u_0^2\psi_{20}^2 + 3g_{m24b}u_0^2\psi_{40}^2)\,\delta u + \\ &+\left(2g_{m23b}u_0^3\psi_{20} + 2g_{m24b}u_0^3\psi_{20}\right)\delta\psi_2 + \\ &+\left(g_{mpb}\right)\delta\dot{\psi}_2 + \left(-2g_{m23b}u_0^3\psi_{30}\right)\delta\psi_3 + \\ &+\left(-2g_{m24b}u_0^3\psi_{40}\right)\delta\psi_4 + \left(g_{mVb}\right)\delta\dot{u}\end{aligned} \quad (14)$$

where the zero indices indicate the steady-state values of the quantities.

Omitting the signs of variations, the resulting expression is written in abbreviated form using the time differentiation operator $p = d/dt$:

$$\begin{aligned}&\left(T_1 p + 1\right)\psi_2 = \\ &= -k_\psi\left(T_2 p + 1\right)u + C_1\psi_1 + C_3\psi_3 + C_4\psi_4 + C_0\Omega\end{aligned} \quad (15)$$

Hereafter, T_i, C_i, k_ψ and Y_i are the time and geometric constants obtained after linearization, depending on the steady–state values of $\psi_{10}, \psi_{20}, \psi_{30}, \psi_{40}$, as well as u_0 and Ω_0.

The equation of dynamics of the automatic regulator can be obtained by linearizing (13) and combining it with (15). Then the expression for the dimensionless load on the movable ring φ:

$$\begin{aligned}&(T_1 p + 1)\varphi = \\ &= -k_\psi Y_2\left(T_2 p + 1\right)u + Y_3\left(T_1 p + 1\right)\psi_3 + \\ &+ Y_4\left(T_1 p + 1\right)\psi_4 + C_1 Y_2\psi_1 + C_3 Y_2\psi_3 + \\ &+ C_4 Y_2\psi_4 + C_0 Y_2\Omega\end{aligned} \quad (16)$$

The equation of axial vibrations of the ring (16) in the operator form has the form:

$$\left(T_3^2 p^2 + T_4 p + \lambda\right)u = \varphi \quad (17)$$

Excluding from (16) and (17) φ, the equation of the dynamics of the system is obtained:

$$\begin{aligned}&D(p)u = \left(a_3 p^3 + a_2 p^2 + a_1 p + a_0\right)u = \\ &= Y_3\left(T_1 p + 1\right)\psi_3 + Y_4\left(T_1 p + 1\right)\psi_4 + \\ &+ C_1 Y_2\psi_1 + C_3 Y_2\psi_3 + C_4 Y_2\psi_4 + C_0 Y_2\Omega\end{aligned} \quad (18)$$

where $a_3 = T_3^2 T_1$, $a_2 = T_3^2 + T_1 T_4$, $a_1 = T_4 + \lambda T_1 + T_2 k$, $a_0 = \lambda + k_\psi$.

3 CONCLUSIONS

The use of a combined approach to create a mathematical model of a gas seal, combining analytical and numerical solutions, made it possible to obtain a convenient tool for studying the operation processes of contactless seals in general and impulse seal in particular.

The considered mathematical model of a gas-barrier impulse face seal makes it possible to design economical and reliable seals with a given barrier gas flow rate for a wide range of operating pressures of the pumped product and shaft speeds. The dynamic characteristics of the seal, set using the presented model, make it possible to determine in advance the range of stable non-contact operation of the seal.

Using this model to study the behavior of the seal in start-up or emergency operating conditions makes it possible to design new types of pumps and compressors with improved safety characteristics. The use of a gas-barrier impulse face seal instead of seals with gas-dynamic grooves on the surfaces of sealing rings makes it possible to significantly reduce the cost of operation and maintenance of centrifugal machines, expand the range of their operating parameters.

ACKNOWLEDGMENTS

This work was supported by the project VEGA 1/0226/21 of Scientific Grant Agency of the Ministry of Education, science, research and sport of the Slovak Republic and the Slovak Academy of Sciences.

REFERENCES

[Adamcik 2014] Adamcik, F., et al. Modeling of Changes in Flow Air Fuel Effected by Changes in Environmental Conditions. Nase More, 2014, Vol. 61, No. 1-2., pp. 40-42. ISSN 0469-6255.

[Balara 2018] Balara, M., Duplakova, D., Matiskova, D. Application of a signal averaging device in robotics. Measurement, 2018, Vol. 115, No. 2, pp. 125-132.

[Baron 2016] Baron, P., Dobransky, J., Kocisko, M., Pollak, M., Cmorej, T. The parameter correlation of acoustic emission and high-frequency vibrations in the assessment process of the operating state of the technical system. Acta Mechanica et Automatica, 2016, Vol. 10, No. 2, pp. 112-116.

[Catlos 2018] Catlos, M., et al. Continual Monitoring of Precision of Aerial Transport Objects. In: 13th Int. Sci. Conf. on New Trends in Aviation Development (NTAD); Kosice, 30-31 August 2018. New York: IEEE, pp. 30-34. ISBN 978-1-5386-7918-0.

[Chaus 2018] Chaus, A.S., Pokorny, P., Caplovic, E., Sitkevich, M.V., Peterka, J. Complex fine-scale diffusion coating formed at low temperature on high-speed steel substrate. Applied Surface Science, 2018, Vol. 437, pp. 257-270. ISSN 0169-4332.

[Duplakova 2018] Duplakova, D., et al. Determination of optimal production process using scheduling and simulation software. International J. of Simulation Modelling, 2018, Vol. 17, No. 4, p. 447.

[Flegner 2019] Flegner, P., Kacur, J., Durdan, M., Laciak, M. Processing a measured vibroacoustic signal for rock type recognition in rotary drilling technology. Measurement, 2019, Vol. 134, pp. 451-467.

[Flegner 2020] Flegner, P., Kacur, J., Durdan, M, Laciak, M. Statistical Process Control Charts Applied to Rock Disintegration Quality Improvement. Applied sciences, 2020, Vol. 10, No. 23, pp. 1-26.

[Gamec 2019] Gamec, J., et al. Low Profile Sinuous Slot Antenna for UWB Sensor Networks. Electronics, 2019, Vol. 8, No. 2, pp. 1-11. ISSN 2079-9292.

[Harnicarova 2019] Harnicarova, M., et al. Study of the influence of the structural grain size on the mechanical properties of technical materials.

Materialwissenschaft und Werkstofftechnik, 2019, Vol. 50, No. 5, pp. 635-645.

[Jurko 2011] Jurko, J., Gajdos, M., Panda, A. Study of changes under the machined surface and accompanying phenomena in the cutting zone during drilling of stainless steels with low carbon content. Metalurgija, 2011, Vol. 50, No. 2, pp. 113-117.

[Kuznetsov 2019] Kuznetsov E., Panda A., Nahornyi V., et al. Experimental Researches of the Pulse Gas barrier Face Seal. MM Science J., 2019, No. December, pp. 3519-3523.

[Kuznetsov 2020] Kuznetsov E., Nahornyi V., Krenicky T. Gas Flow Simulation In The Working Gap of Impulse Gas-Barrier Face Seal. Management Systems in Production Engineering, 2020, Vol. 28, Issue 4, pp. 298-303. DOI: DOI 10.2478/mspe-2020-0042.

[Kuznetsov 2023] Kuznetsov E., Pandova I. Calculation of the Operational Characteristics of the Impulse Gas-Barrier Face Seal. Manag. Systems in Production Engineering, 2023, Vol. 31, Issue 4, pp. 411-417.

[Labun 2018] Labun, J., et al. Possibilities of Increasing the Low Altitude Measurement Precision of Airborne Radio Altimeters. Electronics, 2018, Vol. 7, No. 9., pp. 1-9.

[Macala 2017] Macala, J., Pandova, I., Panda, A. Zeolite as a prospective material for the purification of automobile exhaust gases. Mineral Resources Management, 2017, Vol. 33, No. 1, pp. 125-137.

[Michalik 2014] Michalik, P., Zajac, J., Hatala, M., Mital, D. and Fecova, V. Monitoring surface roughness of thin-walled components from steel C45 machining down and up milling. Measurement, 2014, Vol. 58, pp. 416-428, ISSN 0263-2241.

[Monkova 2013] Monkova, K., Monka, P., Jakubeczyova, D. The research of the high speed steels produced by powder and casting metallurgy from the view of tool cutting life. Applied Mechanics and Materials, 2013, Vol. 302, pp. 269-274.

[Mrkvica 2016] Mrkvica, I., Neslusan, M., Cep, R., Sléha, V. Properties and comparison of PVD coatings. Technical Gazette, 2016, Vol. 23, No. 2, pp. 569-574.

[Murcinkova 2019] Murcinkova, Z., et al. Damping properties of fibre composite and conventional materials measured by free damped vibration response. Advances in Mechanical Engineering, Vol. 11, No. 5.

[Olejarova 2017] Olejarova, S., Dobransky, J., Svetlik, J., Pituk, M. Measurements and evaluation of measurements of vibrations in steel milling process. Measurement, 2017, Vol. 106, pp. 18-25.

[Olejarova 2021] Olejarova, S. and Krenicky, T. Water Jet Technology: Experimental Verification of the Input Factors Variation Influence on the Generated Vibration Levels and Frequency Spectra. Materials, 2021, Vol. 14, 4281.

[Panda 2014] Panda, A., Prislupcak, M., Pandova, I. Progressive technology diagnostics and factors affecting machinability. Applied Mechanics and Materials, 2014, Vol. 616, pp. 183-190.

[Panda 2021] Panda, A., et al. Increasing of wear resistance of linear block-polyurethanes by thermal processing methods. MM Science J., 2021, Vol. October, pp. 4731-4735.

[Pandova 2018] Pandova, I., et al. Use of sorption of copper cations by clinoptilolite for wastewater treatment. Int. J. of Environmental Research and Public Health, 2018, Vol. 15, No. 7, 1364.

[Pandova 2020] Pandova, I., et al. A study of using natural sorbent to reduce iron cations from aqueous solutions. Int. J. of Environmental Research and Public Health, 2020, Vol. 17, No. 10, 3686.

[Pollak 2019] Pollak, M., Kascak, J., Teliskova, M., Tkac, J. Design of the 3D printhead with extruder for the implementation of 3D printing from plastic and recycling by industrial robot. TEM Journal, 2019, Vol. 8, No. 3, pp. 709-713.

[Pollak 2020] Pollak, M., Torokova, M., Kocisko, M. Utilization of generative design tools in designing components necessary for 3D printing done by a robot. TEM Journal, 2020, Vol. 9, No. 3, pp. 868-872.

[Rimar 2016] Rimar, M., Smeringai, P., Fedak M., Kuna S. Technical and software equipment for the real time positioning control system in mechatronic systems with pneumatic artificial muscles. Key Engineering Materials, 2016, Vol. 669, pp. 361-369.

[Sedlackova 2017] Sedlackova, N.A, et al. Synthesis Criterion of Ergatic Base Complex with Focus on its Reliability. In: 14th IEEE International Scientific Conference on Informatics, Poprad, 14-19 November 2017. New York: IEEE, pp 318-321. ISBN 978-1-5386-0889-0.

[Straka 2021] Straka, L., Pitel, J. and Corny, I. Influence of the main technological parameters and material properties of the workpiece on the geometrical accuracy of the machined surface at WEDM. Inter. J. of Advanced Manuf. Technology, 2021, Vol. 115, No. 9-10, pp. 3065-3087.

[Straka 2022] Straka, L., Gombar, M., Vagaska, A., Kuchta, P. Efficiency Optimization of the Electroerosive Process in μ-WEDM of Steel MS1 Sintered Using DMLS Technology. Micromachines, 2022, Vol. 13, 1446.

[Sukhodub 2018] Sukhodub, L., Panda, A., Dyadyura, K., Pandova, I., Krenicky, T. The design criteria for biodegradable magnesium alloy implants. MM Science J., 2018, Vol. December, pp. 2673-2679.

[Sukhodub 2019] Sukhodub, L., et al. Hydroxyapatite and zinc oxide based two-layer coating, deposited on Ti6Al4V substrate. MM Science J., Vol. December, pp. 3494-3499.

[Svetlik 2014] Svetlik, J., Baron, P., Dobransky, J., Kocisko, M. Implementation of Computer System for Support of Technological Preparation of Production for Technologies of Surface Processing. Applied Mechanics and Materials, 2014, Vol. 613, p. 418.

[Vagaska 2021] Vagaska, A., Gombar, M. Mathematical Optimization and Application of Nonlinear Programming. Studies in Fuzziness and Soft Computing, 2021, Vol. 404, Iss. 2021, pp. 461-486.

[Zaborowski 2007] Zaborowski, T. Ekowytwarzanie. Gorzow, 2007, 100 p.

CONTACTS:

Prof. Eng. Anton Panda, PhD.
Faculty of Manufacturing Technologies with a seat in Presov
Technical University of Kosice, Slovakia
Sturova 31, 080 001 Presov, Slovakia
e-mail: anton.panda@tuke.sk